Advanced Composite Materials
Publication details, including instructions for authors and subscription information:
http://www.tandfonline.com/loi/tacm20

Analysis of Thermoelastic Characteristics of a Rotating FGM Circular Disk by Finite Element Method

J. Go [a] , A. M. Afsar [b] & J. I. Song [c]

[a] Department of Mechanical Engineering, Changwon National University, 9 Sarim Dong, Changwon Si, Gyeongnam 641-773, South Korea

[b] Department of Mechanical Engineering, Changwon National University, 9 Sarim Dong, Changwon Si, Gyeongnam 641-773, South Korea;, Email: mdafsarali1967@yahoo.com

[c] Department of Mechanical Engineering, Changwon National University, 9 Sarim Dong, Changwon Si, Gyeongnam 641-773, South Korea

Version of record first published: 02 Apr 2012.

To cite this article: J. Go , A. M. Afsar & J. I. Song (2010): Analysis of Thermoelastic Characteristics of a Rotating FGM Circular Disk by Finite Element Method, Advanced Composite Materials, 19:2, 197-213

To link to this article: http://dx.doi.org/10.1163/092430410X490473

VSP

Advanced Composite Materials 19 (2010) 197–213

ADVANCED COMPOSITE MATERIALS
brill.nl/acm

Analysis of Thermoelastic Characteristics of a Rotating FGM Circular Disk by Finite Element Method

J. Go, A. M. Afsar * and J. I. Song

Department of Mechanical Engineering, Changwon National University, 9 Sarim Dong, Changwon Si, Gyeongnam 641-773, South Korea

Received 5 December 2008; accepted 15 June 2009

Abstract

This study concerns the analysis of thermoelastic characteristics of a thin circular functionally graded material (FGM) rotating disk having a concentric hole and subjected to a thermal load. The Young's modulus, coefficient of thermal expansion (CTE), and density of the disk are assumed to vary exponentially in the radial direction only while the Poisson's ratio is assumed to be constant. The incompatible eigenstrain developed in the FGM disk due to nonuniform coefficient of thermal expansion and change in temperature is taken into account. Based on the two-dimensional thermoelastic theories, the axisymmetric problem is reduced to the solution of a second-order ordinary differential equation. Using the variational approach and Ritz method, a finite element model is developed for numerical solution of the problem. The model is verified for a homogeneous circular rotating disk and demonstrated for an Al_2O_3/Al FGM disk. Some numerical results of thermoelastic field in the Al_2O_3/Al FGM disk are presented and discussed. It is found that the thermoelastic characteristics of an FGM disk are largely dependent on temperature distribution profile, radial thickness of the disk, angular speed of the disk, and the inner and outer surface temperature difference, and can be controlled by controlling these parameters.

Keywords

Functionally graded material, thermoelasticity, circular disk, eigenstrain, finite element method, circular cutter

1. Introduction

Functionally graded materials (FGMs) consist of two or more distinct material phases whose volume fractions continuously vary with space variables. Consequently, these materials have continuously varying mechanical and thermal properties. Usually, a ceramic is used at one surface to resist severe environmental effects, such as high temperature, wear, and corrosion, and a metal is used at the other surface to ensure high toughness and thermal conductivity. Therefore, an FGM is

* To whom correspondence should be addressed. E-mail: mdafsarali1967@yahoo.com
Edited by the KSCM

 DOI:10.1163/092430410X490473

a promising candidate for many engineering applications where a high temperature gradient field is the main concern. The original purpose of these materials was to develop thermal barrier coatings for the propulsion system of space-planes to resist high temperature and ensure high thermal conductivity at the same time [1]. However, their unique properties have stimulated the interests of researchers towards the development of new potential structural and functional applications. Therefore, these materials are being still studied constantly to explore their characteristics from different points of view.

For potential applications as structural elements, FGM beams, plates, shells, and cylinders have been studied extensively for different geometries under different loading conditions. Yongdong *et al.* [2] and Zhong and Yu [3] considered FGM beams of rectangular cross-section for the analysis of stress due to mechanical loads. Thermal load was considered by Xiang and Yang [4] for the analysis of free and forced vibration of a laminated functionally graded Timoshenko beam of variable thickness. A Timoshenko beam of FGMs was also considered to investigate the post-buckling behavior in response to the thermal load [5]. FGM beams have been considered not only for stress, vibration, and buckling analyses but also for the analysis of fracture behavior [6].

Chen and Liew [7] and Feldman and Aboudi [8] analyzed buckling characteristics of rectangular FGM plates in response to nonlinearly distributed in-plane edge loads and uniaxial load, respectively. Assuming the material properties to be varied in the thickness direction according to the sigmoid function, geometrically nonlinear analysis was carried out for FGM plates and shells by Kim *et al.* [9]. The solutions of axisymmetric bending and buckling of an FGM circular plate based on third-order plate theory and classical plate theory have been discussed by Ma and Wang [10]. In our previous study [11], an FGM rectangular plate under mechanical load was considered with a view to examining the effect of nonhomogeneous parameters on the elastic field. Chung and Chang [12] also considered an FGM rectangular plate to study the mechanical behavior of the plate subjected to thermal loadings.

FGM circular cylinder and hollow sphere were considered by Obata and Noda [13] to carry out the analysis of thermal stresses. A similar study was carried out by Liew *et al.* [14] to investigate the thermal stress behavior of an FGM circular cylinder. As the FGMs have continuously varying coefficient of thermal expansion, an eigenstrain [15] is inherently developed in the materials when they undergo a change in temperature. The incompatibility of this eigenstrain causes an eigenstress or thermal residual stress to develop in these materials. Thus, the incompatible eigenstrain is an important issue to be considered in characterizing the FGM bodies. By taking into account the effect of incompatible eigenstrain, Afsar and Sekine [16], Afsar and Anisuzzaman [17], and Afsar *et al.* [18] analyzed the brittle fracture characteristics of thick-walled FGM cylinders.

Among other geometries of FGM bodies, a rotating FGM hollow shaft with fixed ends was chosen by Eraslan and Akis [19] for estimating the elastoplastic response

of the shaft and a rotating FGM sandwich solid disk with material gradient in the thickness direction was considered by Zenkour [20] for the analysis of stress and displacement.

It is found from the above discussion that extensive studies on FGMs have been carried out to explore their potential applications mainly as structural elements like beams, plates, shells, and cylinders. Studies on FGMs to explore their functional applications in the field of cutting and grinding tools seem to be inadequate in the literatures. Cho and Park [21] have investigated the thermoelastic characteristics of functionally graded lathe cutting tools composed of Cr–Mo steel shank and ceramic tip with a view to exploring their thermomechanical superiority. They found that the thermomechanical stress concentration was significantly relaxed by adding an FGM layer between the steel shank and the ceramic tip and thus justified the potential of FGMs for high performance metal cutting tools.

In this study, attention is focused on the concept of FGMs in the design of a circular disk type cutter or a grinding disk. A circular cutter or a grinding disk experiences a higher temperature at the cutting edge or grinding surface when it rotates and comes in contact with an object, and a lower temperature at the central region of the disk. Further, the cutting edge or grinding surface of the tool should be harder and have high wear resistance while the central part should have a higher toughness. A uniform material or bi-materials cannot meet these requirements because a high thermal stress is developed in the case of a uniform or bi-materials that causes failure. However, these requirements of a disk can be met up by designing the disk with the concept of FGMs. This urges one to understand, quantify, and improve the thermoelastic characteristics of a rotating FGM circular disk which, in turn, requires a suitable analysis model. In an attempt to achieve this goal, this study concentrates on the development of a suitable model and analysis of thermoelastic characteristics of a rotating FGM circular disk with a concentric hole. The incompatible eigenstrain developed in the disk due to nonuniform CTE and the inertia force due to rotation of the disk are taken into account. Here, it is worthwhile to mention that although such a disk type cutter or grinder experiences a contact load when it comes in contact with a work piece, it is not considered in the present study. The solution of the contact problem of an FGM disk can be considered in another study and superposed with the solution of the present thermoelastic problem to obtain the resultant characteristics. The Young's modulus, CTE, and density of the FGM disk are assumed to vary exponentially only in the radial direction while the Poisson's ratio is assumed to be constant [10, 22]. Based on the two-dimensional thermoelastic theories, the problem is reduced to the solution of a second-order differential equation. Using a variational approach and Ritz method, a finite element model is developed to obtain a numerical solution of the problem. The validity of the finite element model is verified for a homogeneous circular rotating disk. Then, the model is demonstrated for an Al_2O_3/Al FGM disk and some numerical results of thermoelastic stresses and strains are presented to examine the effects of temper-

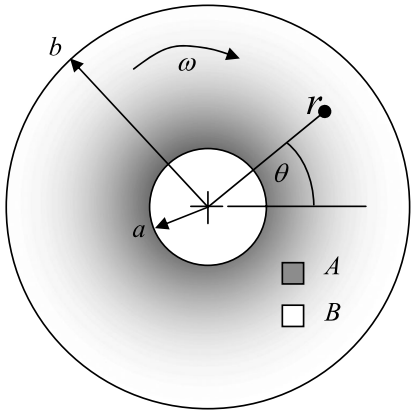

Figure 1. Analytical model of the problem.

ature distribution profile, radial thickness of the disk, angular speed of the disk, and the inner and outer surface temperature difference.

2. Statement of the Problem

With reference to the polar coordinate system r–θ, a rotating FGM circular disk with a circular hole at the center of the disk is shown in Fig. 1. The constituent materials of the FGM disk are denoted by A and B which are, respectively, represented by the dark and white colors as shown in the figure. The distribution of each material continuously varies along the radial direction only. The radii of the hole and the disk are designated by a and b, respectively. Further, the angular velocity of the disk is denoted by ω, which can be determined from the relation $\omega = 2\pi N/60$, where N is the revolutions per minute (rpm). As the material distribution is the function of r only, all the properties of the FGM disk are also functions of r only, which reduces it to the axisymmetric problem. The Young's modulus E, coefficient of thermal expansion α, and the density ρ of the FGM disk are assumed to vary exponentially as:

$$E = E_0 \mathrm{e}^{\beta r}, \tag{1a}$$

$$\alpha = \alpha_0 \mathrm{e}^{\gamma r}, \tag{1b}$$

$$\rho = \rho_0 \mathrm{e}^{\mu r}. \tag{1c}$$

It is noted that the surface of the hole ($r = a$) contains 100% material A whereas the outer surface of the disk ($r = b$) contains 100% material B. Thus, the constants in equation (1) can be determined as:

$$E_0 = E_A \mathrm{e}^{-\beta a}, \tag{2a}$$

$$\alpha_0 = \alpha_A \mathrm{e}^{-\gamma a}, \tag{2b}$$

$$\rho_0 = \rho_A e^{-\mu a}, \tag{2c}$$

$$\beta = \frac{1}{a-b}\ln(E_A/E_B), \tag{3a}$$

$$\gamma = \frac{1}{a-b}\ln(\alpha_A/\alpha_B), \tag{3b}$$

$$\mu = \frac{1}{a-b}\ln(\rho_A/\rho_B). \tag{3c}$$

The subscripts A and B of a variable are used to denote the properties of the constituent materials A and B, respectively, while the non-subscripted variables are used to represent the properties of the FGM composed of the materials A and B. Although the material properties vary continuously from the inner surface to the outer surface of the disk, the properties at a point are assumed to be same at all the directions, i.e., the FGM disk is isotropic. Further, the disk has a small constant thickness. As a result, the analysis falls under the case of the plane stress condition.

3. Thermoelastic Formulation

Eigenstrains [15] are nonelastic strains or free expansion strains that are developed in a body and arise for various reasons, such as phase transformation, precipitation, temperature change, etc. The incompatibility of these eigenstrains produces stresses that should be taken into account along with other loadings in order to obtain the resultant effects. In the present study, the eigenstrain is associated with the thermal expansion as the FGM disk undergoes a change in temperature. Since the material of the FGM disk is isotropic, the thermal eigenstrain at a point is the same in all directions which can be given by

$$\varepsilon^* = \alpha(r)T(r), \tag{4}$$

where $T(r)$ is the change in temperature at any point r. The total strain is the sum of the elastic strain and the eigenstrain. Thus, the components of total strain are given by

$$\varepsilon_r = \mathrm{e}_r + \varepsilon^*, \tag{5a}$$

$$\varepsilon_\theta = \mathrm{e}_\theta + \varepsilon^*, \tag{5b}$$

where ε_r and ε_θ are the radial and circumferential components of the total strain, and e_r and e_θ are the radial and circumferential components of the elastic strain, respectively. It is noted that the shear strain component does not come into the scenario due to the symmetric deformation of the disk. The elastic strains are related to stresses by Hooke's law. Thus,

$$\varepsilon_r = \frac{1}{E}(\sigma_r - \nu\sigma_\theta) + \varepsilon^*, \tag{6a}$$

$$\varepsilon_\theta = \frac{1}{E}(\sigma_\theta - \nu\sigma_r) + \varepsilon^*, \tag{6b}$$

where σ_r and σ_θ are the radial and circumferential stress components, respectively. By considering the inertia force due to the rotation of the disk as the only body force, the two-dimensional equilibrium equations in polar coordinate can be written as:

$$\frac{\partial \sigma_r}{\partial r} + \frac{1}{r}\frac{\partial \tau_{r\theta}}{\partial \theta} + \frac{\sigma_r - \sigma_\theta}{r} + \rho\omega^2 r = 0, \tag{7a}$$

$$\frac{\partial \tau_{r\theta}}{\partial r} + \frac{1}{r}\frac{\partial \sigma_\theta}{\partial \theta} + \frac{2\tau_{r\theta}}{r} = 0. \tag{7b}$$

Because of the symmetry, $\tau_{r\theta}$ vanishes and σ_r, σ_θ are independent of θ. Thus, the second equilibrium equation (equation (7b)) is identically satisfied and the first equilibrium equation (equation (7a)) is reduced to

$$\frac{\mathrm{d}}{\mathrm{d}r}(r\sigma_r) - \sigma_\theta + \rho\omega^2 r^2 = 0. \tag{8}$$

Now, the substitution of

$$F = r\sigma_r \tag{9a}$$

into equations (8) and (6), respectively, gives

$$\sigma_\theta = \frac{\mathrm{d}F}{\mathrm{d}r} + \rho\omega^2 r^2, \tag{9b}$$

$$\varepsilon_r = \frac{1}{E}\left(\frac{F}{r} - \nu\frac{\mathrm{d}F}{\mathrm{d}r}\right) - \frac{\nu\rho}{E}\omega^2 r^2 + \varepsilon^*, \tag{10a}$$

$$\varepsilon_\theta = \frac{1}{E}\left(\frac{\mathrm{d}F}{\mathrm{d}r} - \frac{\nu F}{r}\right) + \frac{\rho\omega^2 r^2}{E} + \varepsilon^*. \tag{10b}$$

To satisfy the compatibility condition between the strain components, we consider the strain–displacement relations which, for the axisymmetric problem, are given by

$$\varepsilon_r = \frac{\mathrm{d}u_r}{\mathrm{d}r}, \tag{11a}$$

$$\varepsilon_\theta = \frac{u_r}{r}. \tag{11b}$$

From these two equations, it is seen that the two strain components are related by $\varepsilon_r = \mathrm{d}/\mathrm{d}r(r\varepsilon_\theta)$. By making use of equation (10) into this relation, one can readily obtain

$$\frac{\mathrm{d}^2 F}{\mathrm{d}r^2} + \left(\frac{1}{r} - \beta\right)\frac{\mathrm{d}F}{\mathrm{d}r} + \frac{1}{r}\left(\beta\nu - \frac{1}{r}\right)F = \rho\omega^2 r(\beta r - \mu r - \nu - 3) - E\alpha\left(\gamma T + \frac{\mathrm{d}T}{\mathrm{d}r}\right). \tag{12}$$

Equation (12) is the governing second-order differential equation. Once this equation is solved for F, the components of stress, strain, and displacement can readily be found from equations (9), (10), and (11), respectively.

4. Finite Element Formulation

As the analytical solution of equation (12) is quite involved, the finite element method is adopted to obtain its numerical solution. Following the variational approach, equation (12) is multiplied by a trial function w and integrated over the domain of the problem to obtain:

$$\int_a^b w\,\frac{\mathrm{d}^2F}{\mathrm{d}r^2}\,\mathrm{d}r + \int_a^b \left(\frac{1}{r}-\beta\right) w\,\frac{\mathrm{d}F}{\mathrm{d}r}\,\mathrm{d}r + \int_a^b \frac{1}{r}\left(\beta\nu - \frac{1}{r}\right) w\,F\,\mathrm{d}r = \int_a^b wf(r)\,\mathrm{d}r,$$

where

$$f(r) = \rho\omega^2 r(\beta r - \mu r - \nu - 3) - E\alpha\left[\gamma T + \frac{\mathrm{d}T}{\mathrm{d}r}\right] \tag{13}$$

integration by parts yields

$$\begin{aligned}\int_a^b \frac{\mathrm{d}w}{\mathrm{d}r}\frac{\mathrm{d}F}{\mathrm{d}r}\,\mathrm{d}r - \int_a^b \left(\frac{1}{r}-\beta\right) w\,\frac{\mathrm{d}F}{\mathrm{d}r}\,\mathrm{d}r - \int_a^b \frac{1}{r}\left(\beta\nu - \frac{1}{r}\right) wF\,\mathrm{d}r \\ = -\int_a^b wf(r)\,\mathrm{d}r + w(b)\,\frac{\mathrm{d}F}{\mathrm{d}r}(b) - w(a)\,\frac{\mathrm{d}F}{\mathrm{d}r}(a).\end{aligned} \tag{14}$$

For the present rotating disk problem, the following boundary conditions apply

(i) $r = a, \sigma_r = 0$, i.e., $F(a) = 0$,

(ii) $r = b, \sigma_r = 0$, i.e., $F(b) = 0$.

It is seen that both the boundary conditions are essential and homogeneous. The function w must satisfy these boundary conditions.

Now, the radial domain of the disk $\Omega = (a, b)$ is divided into N number of subdomains $\Omega^e = (r_e, r_{e+1})$, where $e = 1, 2, \ldots, N$. Since equation (14) is valid throughout the domain Ω, it is valid in all the subdomains Ω^e. Thus, the variational form of equation (14) is:

$$B(w, F) = l(w), \tag{15}$$

where

$$\begin{aligned}B(w, F) = \int_{r_e}^{r_{e+1}} \frac{\mathrm{d}w}{\mathrm{d}r}\frac{\mathrm{d}F}{\mathrm{d}r}\,\mathrm{d}r - \int_{r_e}^{r_{e+1}} \left(\frac{1}{r}-\beta\right) w\,\frac{\mathrm{d}F}{\mathrm{d}r}\,\mathrm{d}r \\ - \int_{r_e}^{r_{e+1}} \frac{1}{r}\left(\beta\nu - \frac{1}{r}\right) wF\,\mathrm{d}r,\end{aligned} \tag{16a}$$

$$l(u) = -\int_{r_e}^{r_{e+1}} wf(r)\,\mathrm{d}r + w(r_{e+1})\,\frac{\mathrm{d}F}{\mathrm{d}r}(r_{e+1}) - w(r_e)\,\frac{\mathrm{d}F}{\mathrm{d}r}(r_e). \tag{16b}$$

The solution is assumed in the form of

$$F = \sum_{j=1}^{2} F_j^e \phi_j^e, \tag{17}$$

where

$$\phi_1^e = \frac{r_{e+1} - r}{r_{e+1} - r_e}, \tag{18a}$$

$$\phi_2^e = \frac{r - r_e}{r_{e+1} - r_e}. \tag{18b}$$

Applying the Ritz method, equation (15) can be written as:

$$\sum_{j=1}^{2} K_{ij}^e F_j^e = L_i^e, \tag{19}$$

where

$$K_{ij}^e = B(\phi_i^e, \phi_j^e), \tag{20a}$$

$$L_i^e = l(\phi_i^e). \tag{20b}$$

Equation (19) is a system of algebraic equations, which can be used to form a global system of algebraic equations by satisfying the continuity condition $F_2^e = F_1^{e+1}$. The global system of algebraic equations is then solved by the Gauss elimination method. The solution of equation (19) gives the discrete values of F at the global node points which are used in equation (17) to compute F at any intermediate points. By making use of equations (9), (10), and (11b), the components of stress, strain, and displacement are then obtained as:

$$\sigma_r = \frac{1}{r} \sum_{j=1}^{2} F_j^e \phi_j^e, \tag{21a}$$

$$\sigma_\theta = \sum_{j=1}^{2} F_j^e \frac{\mathrm{d}\phi_j^e}{\mathrm{d}r} + \rho\omega^2 r^2, \tag{21b}$$

$$\varepsilon_r = \frac{1}{E} \sum_{j=1}^{2} \left[\frac{F_j^e \phi_j^e}{r} - \nu F_j^e \frac{\mathrm{d}\phi_j^e}{\mathrm{d}r} \right] - \frac{\nu\rho\omega^2 r^2}{E} + \varepsilon^*, \tag{22a}$$

$$\varepsilon_\theta = \frac{1}{E} \sum_{j=1}^{2} \left[F_j^e \frac{\mathrm{d}\phi_j^e}{\mathrm{d}r} - \frac{\nu}{r} F_j^e \phi_j^e \right] + \frac{\nu\rho\omega^2 r^2}{E} + \varepsilon^*, \tag{22b}$$

$$u_r = \frac{r}{E} \sum_{j=1}^{2} \left[F_j^e \frac{\mathrm{d}\phi_j^e}{\mathrm{d}r} - \frac{\nu}{r} F_j^e \phi_j^e \right] + \frac{\nu\rho\omega^2 r^3}{E} + r\varepsilon^*. \tag{23}$$

Here, it is noted that the present finite element model can be applied to a homogeneous circular rotating disk by setting the parameters $\beta = \gamma = \mu = 0$.

5. Results and Discussion

In this section, some numerical results of different components of stress and strain are presented for an Al_2O_3/Al FGM disk in which the ingredient materials Al and Al_2O_3 correspond to A and B, respectively. The mechanical and thermal properties of these ingredient materials are shown in Table 1. The Poisson's ratio of the FGM disk is taken as 0.3, which is kept constant throughout the material. To verify the validity of the present finite element model, it is applied to the case of a homogeneous isotropic disk of Al to obtain the components of displacement and stress due to rotation only, without considering any thermal load. The results are compared with the analytical solution obtained by Timoshenko and Goodier [23]. It is noted that the present finite element model can be applied to the homogeneous disk under rotation only by setting the parameters $\beta = \gamma = \mu = 0$ and $\varepsilon^* = 0$. The comparison of the displacement and stress components corresponding to $b/a = 10$ and the angular speed $N = 150$ rpm are presented in Figs 2 and 3, respectively. It is noted that the results agree well within the acceptable limit. The maximum difference is 2.5%, which is found to occur in the displacement at the outer surface of the disk. This small discrepancy in the results is attributed to the inherent error in numerical

Table 1.
Mechanical and thermal properties of Al and Al_2O_3

Materials	Properties		
	Young's modulus (MPa)	Coefficient of thermal expansion (/°C)	Density (g/cm^3)
Al	71	23.1×10^{-6}	2.70
Al_2O_3	380	8.0×10^{-6}	0.96

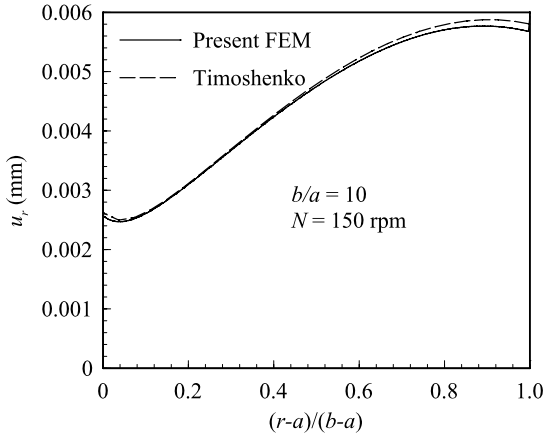

Figure 2. Comparison of radial displacement in a homogeneous circular disk under rotation.

calculations by the finite element model. Thus, it is verified that the present finite element model is capable of producing reliable results with high accuracy.

As all the parameters of interest are only a function of the radial distance of the disk, the disk is meshed in the radial direction only with uniform distribution and equal size of the elements. The dependence of the element size on the results is examined for a disk of inner and outer radii of $a = 15$ mm and $b = 150$ mm, respectively. As all the components of stress, strain, and displacement are computed from the parameter F, the convergence test is carried out only for F. It is obvious that the convergence of F ensures the convergence of the stress, strain, and displacement. Figure 4 shows the convergence criterion of F over the entire radial thickness of the disk. It is noted that the value of F converges very well for the element size of

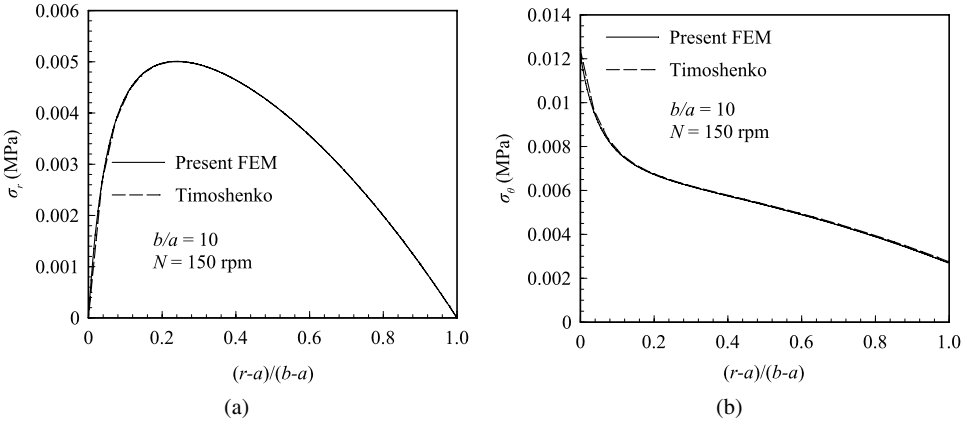

Figure 3. Comparison of stress components in a homogeneous circular disk under rotation; (a) radial, (b) circumferential.

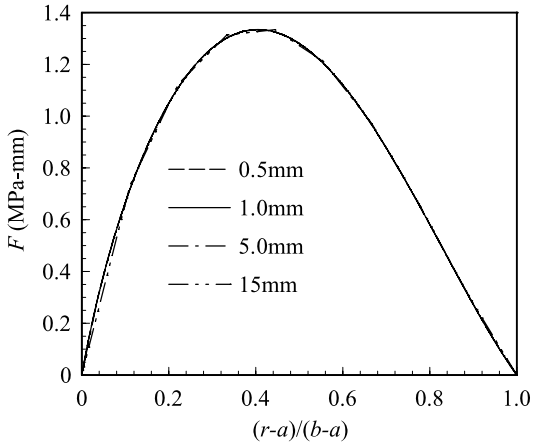

Figure 4. Effect of element size on the parameter F.

5 mm. However, all the results presented in this section correspond to the element size of 1 mm which is chosen to ensure further accuracy of the results.

To examine the effect of temperature distributions on the components of stress and strain, three different prescribed profiles of temperature distribution as a function of normalized radial distance of the disk are considered as shown in Fig. 5. The three temperature distribution profiles are: linear, parabolic, and exponential profiles. It is worthwhile to mention that the present FE model is valid for any temperature distributions for the analysis of thermoelastic characteristics. However, the temperature distributions shown in Fig. 5 are selected as some examples. These temperature distributions can be reasonably expected in an actual grinding disk as a grinding disk or cutter experiences a higher temperature at the grinding (outer) surface and a lower temperature (reasonably room temperature) at the inner surface with a continuous variation of temperature from the outer to the inner surface of the disk. Thus, the actual temperature distribution in a grinding disk can be represented by one of the temperature distributions shown in Fig. 5. For the prescribed temperature distributions in Fig. 5, the corresponding results of stress and strain are presented in Figs 6 and 7, respectively, for the parameters $N = 150$ rpm and $b/a = 10.0$. Shown in Fig. 6(a) are the radial stress distributions from which it is seen that the parabolic temperature distribution yields a compressive radial stress at the outer region and a tensile radial stress at the inner region of the disk. On the other hand, the linear and exponential temperature distributions produce tensile radial stress throughout the entire disk. However, for any temperature distribution, the radial stress is zero at the inner ($(r-a)/(b-a) = 0$) and outer ($(r-a)/(b-a) = 1.0$) surfaces of the disk to satisfy the boundary conditions of the problem. Further, it is noted that the maximum magnitude of the radial stress is obtained for the exponential temperature distribution. The circumferential stress component as shown in Fig. 6(b) has different characteristics from those of the radial stress component.

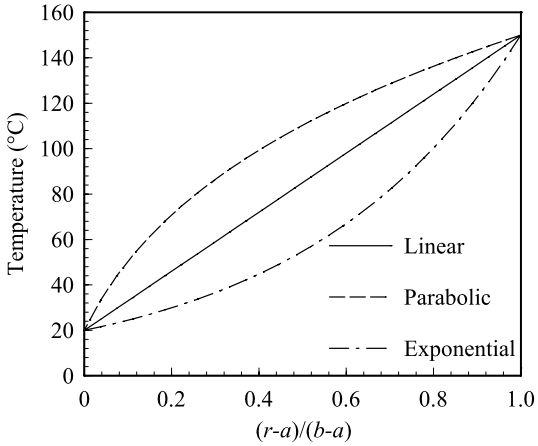

Figure 5. Prescribed temperature distribution profiles along the radial direction of the disk.

For any temperature distribution, the circumferential stress is compressive over a part of the disk and tensile over the other part of the disk. For parabolic temperature distribution, the stress is tensile at and near the inner and outer surfaces of the disk and compressive over the middle region of the disk. The other two temperature distributions (linear and exponential) develop tensile stress over the inner region and compressive stress over the outer region of the disk. As before, the maximum magnitude of the circumferential stress is obtained for the case of exponential temperature distribution. However, the maximum circumferential stress occurs at the outer surface of the disk. Figure 7(a) and 7(b) illustrates the distributions of radial strain and circumferential strain, respectively, for the prescribed temperature distributions of Fig. 5 and $N = 150$ rpm, $b/a = 10.0$. For any temperature distribution, the radial strain component as seen from Fig. 7(a) has the minimum value at the inner surface and then rapidly increases towards the outer surface over the inner region of the disk. On the contrary, the circumferential strain component has the

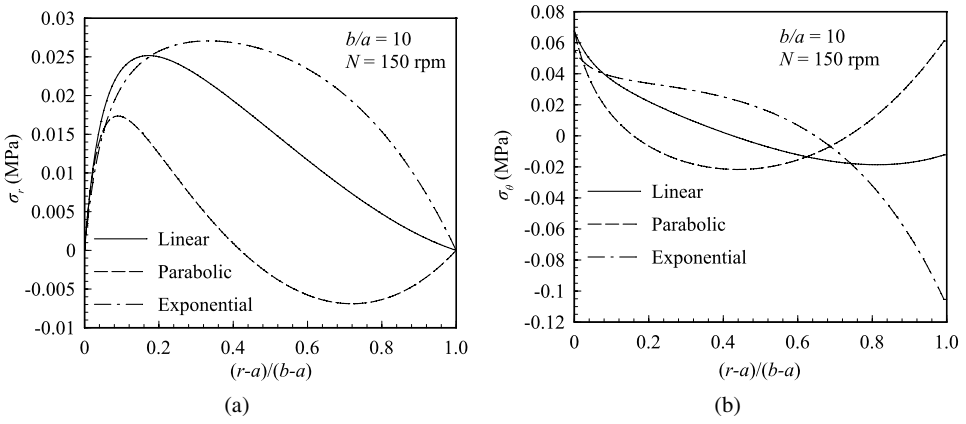

Figure 6. Effect of temperature distribution on the components of stress; (a) radial, (b) circumferential.

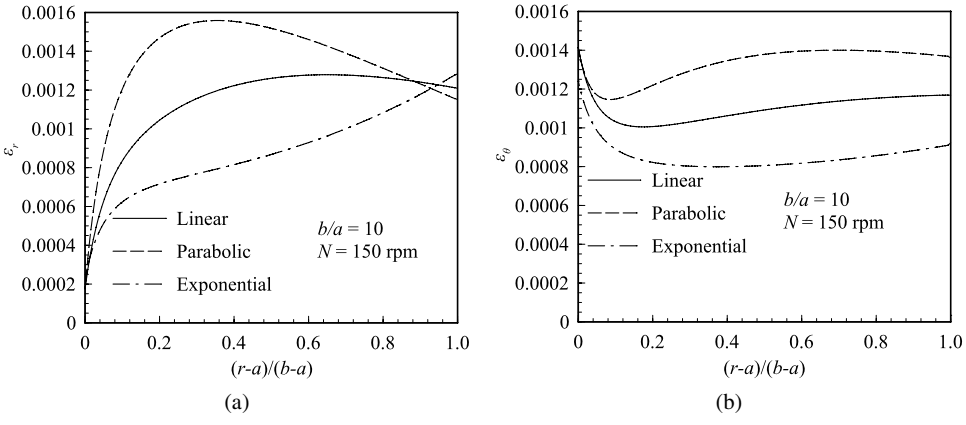

Figure 7. Effect of temperature distribution on the components of strain; (a) radial, (b) circumferential.

maximum value at the inner surface then decreases over the inner region of the disk with r. However, both the strain components have the maximum magnitude for the parabolic temperature distribution.

For the linear temperature distribution of Fig. 5 and angular speed $N = 150$ rpm, the components of stress and strain are plotted in Figs 8 and 9, respectively, for different values of the ratio b/a to investigate the effects of the radial thickness on the results. The value of the ratio b/a is the measure of the radial thickness of the disk. If it is imagined that the outer radius b is constant and the inner radius a is varied, the radial thickness decreases as the ratio b/a decreases (a increases) and *vice versa*. As the radial thickness decreases, the maximum value of the radial stress decreases. In other words, the magnitude of the radial stress increases with the decreases of the size of the hole at the center of the disk. Further, the position of the peak value of the stress moves towards the outer surface as the hole size increases. The nature of the distribution of the circumferential stress as a function

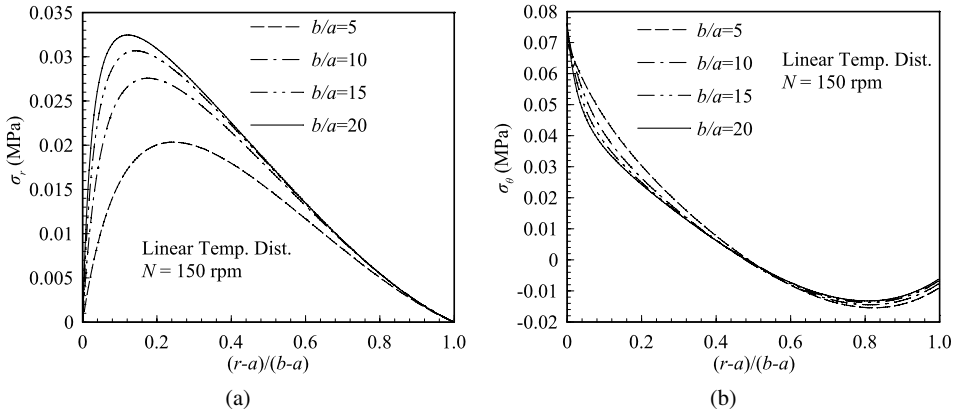

Figure 8. Effect of radial thickness on the components of stress; (a) radial, (b) circumferential.

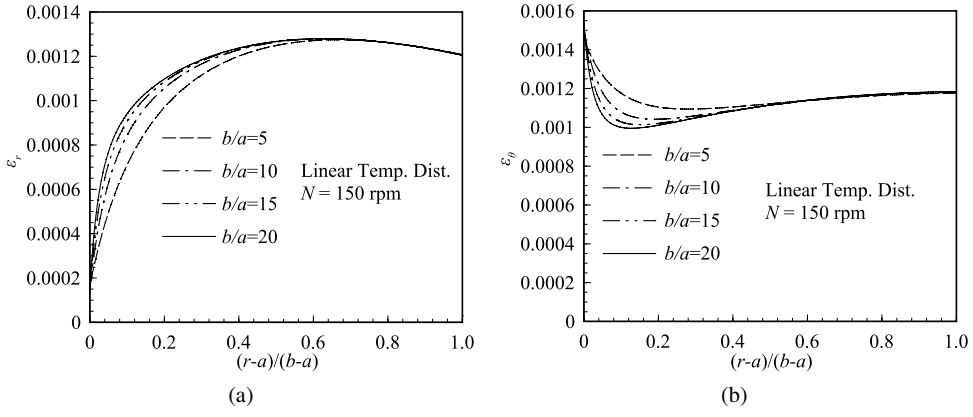

Figure 9. Effect of radial thickness on the components of strain; (a) radial, (b) circumferential.

of b/a is shown in Fig. 8(b). The magnitude of the circumferential stress increases with the increase of the hole size (decrease of b/a), which shows the reverse trend from that of the radial stress component. Figure 9(a) and 9(b) illustrates the effect of radial thickness on the radial and circumferential strain components, respectively. Although the outer region of the disk has almost the same magnitude of strain, there is a considerable variation of strains at the inner region of the disk with the variation of the radial thickness. In this region, the radial strain increases and the circumferential strain decreases as the radial thickness increases, i.e., the hole size decreases.

Figures 10 and 11 illustrate the effects of angular speed — centrifugal force in other words — on the distribution of stress and strain, respectively. The results correspond to the radial thickness $b/a = 10$ and linear temperature distribution of Fig. 5. Four different values of the angular speed $N = 200$, 600, 1000, and 1500 rpm have been considered. A higher angular speed develops a higher centrifugal force.

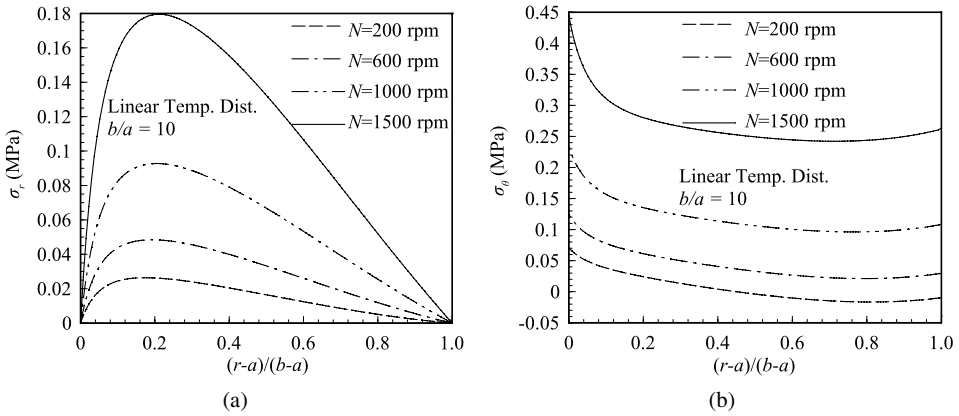

Figure 10. Effect of angular speed on the components of stress; (a) radial, (b) circumferential.

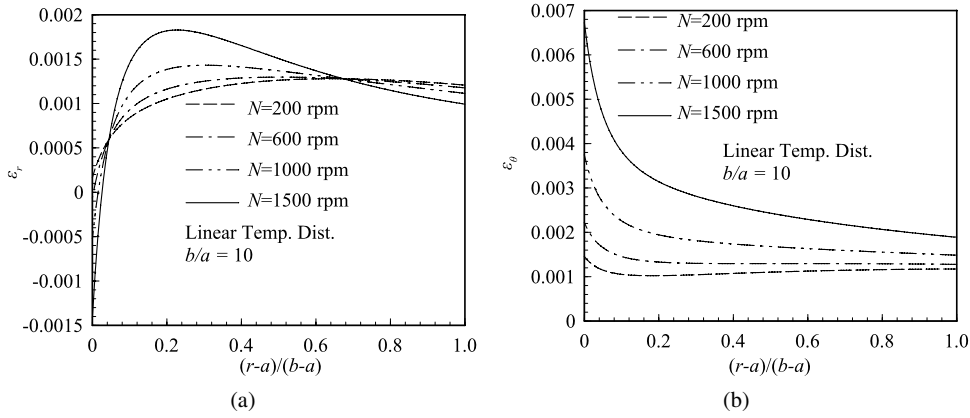

Figure 11. Effect of angular speed on the components of strain; (a) radial, (b) circumferential.

Therefore, the disk experiences the greater radial and circumferential stresses with the rising value of the angular speed, as elucidated in Fig. 10(a) and 10(b). Due to the same reason, the strain components also have a higher value for a higher angular speed as illustrated in Fig. 11(a) and 11(b). However, the radial strain component shown in Fig. 11(a) shows somewhat different characteristics. Over the region of $0.04 < (r-a)/(b-a) < 0.64$, the radial strain increases with the increases of the angular speed. Over the regions of $(r-a)/(b-a) < 0.04$ and $(r-a)/(b-a) > 0.64$, the radial strain has the reverse characteristics, i.e., the radial strain decreases as the angular speed increases.

The temperature of the grinding surface of a disk is in fact not constant. Rather, it varies depending on the speed, contact time, material of work piece, etc. Thus, the effect of the grinding surface temperature on the distribution of stress and strain is analyzed and presented in Figs 12 and 13 for $b/a = 10$, $N = 150$ rpm, and linear temperature profile of Fig. 5. Keeping the inner surface temperature constant

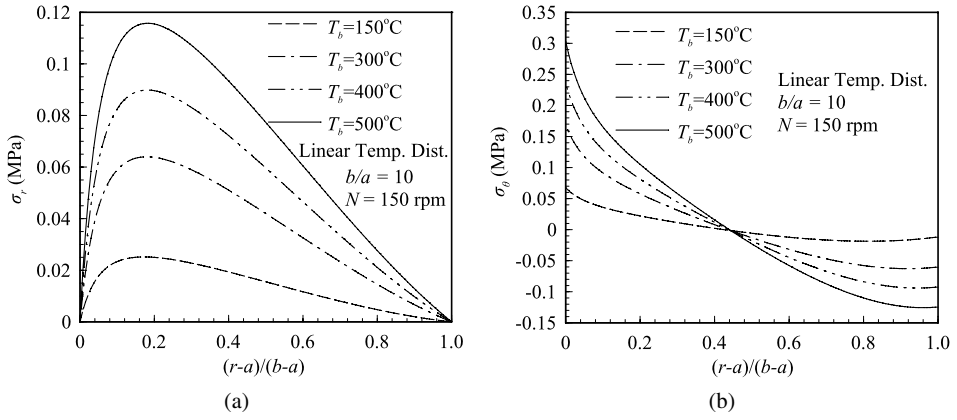

Figure 12. Effect of temperature difference on the components of stress; (a) radial, (b) circumferential.

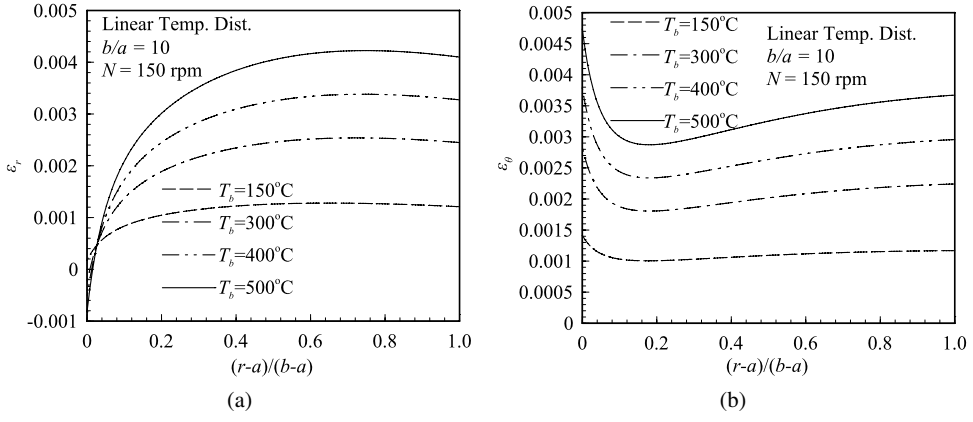

Figure 13. Effect of temperature difference on the components of strain; (a) radial, (b) circumferential.

(20°C), the outer surface (grinding surface) temperature is varied to 150, 300, 400, and 500°C. It is found that the magnitude of all the components of stress and strains increases as the outer surface temperature is increased. This agrees with the obvious fact that the disk will encounter a more critical situation under the case of a higher temperature difference.

6. Conclusions

A finite element model has been developed to analyze the thermoelastic characteristics of a rotating FGM circular disk with a concentric hole. The validity of the model is verified by comparing the results obtained for a disk of homogeneous isotropic material. Then, it is demonstrated for an Al_2O_3/Al FGM disk, and numerical results of different components of stress and strain have been presented. It is found that the thermoelastic characteristics of an FGM disk are largely dependent on the temperature distribution profile, radial thickness, angular speed, and inner and outer surface temperature difference. The thermoelastic characteristics can be controlled by controlling these parameters. Thus, the finite element model developed in this study can be used in designing of an FGM circular cutter or grinding disk to ensure proper and reliable thermoelastic characteristics in service.

Acknowledgement

This work was supported by the Korea Research Foundation (KRF) grant funded by the Korea government (MEST) (No. KRF 2009-0076450). Also, the partial support of the Brain Korea 21 (BK-21) Projects Corps. of the second stage is gratefully acknowledged.

References

1. J. B. Holt, M. Koizumi, T. Hirai and Z. A. Munir, *Ceramic Transactions: Functionally Gradient Materials*, Vol. 34. The American Ceramic Society, Westerville, Ohio, USA (1993).
2. L. Yongdong, Z. Hongcai, Z. Nan and D. Yao, Stress analysis of functionally gradient beam using effective principal axes, *Intl J. Mech. Mater. Des.* **2**, 157–164 (2005).
3. Z. Zhong and T. Yu, Analytical solution of a cantilever functionally graded beam, *Compos. Sci. Technol.* **67**, 481–488 (2007).
4. H. J. Xiang and J. Yang, Free and forced vibration of a laminated FGM Timoshenko beam of variable thickness under heat conduction, *Composites Part B* **39**, 292–303 (2008).
5. S.-R. Li, J.-H. Zhang and Y.-G. Zhao, Thermal post-buckling of functionally graded material Timoshenko beams, *Appl. Math. Mech.* **27**, 803–810 (2006).
6. A. K. Upadhyay and K. R. Y. Simha, Equivalent homogeneous variable depth beams for cracked FGM beams: compliance approach, *Intl J. Fract.* **144**, 209–213 (2007).
7. X. L. Chen and K. M. Liew, Buckling of rectangular functionally graded material plates subjected to nonlinearly distributed in-plane edge loads, *Smart Mater. Struct.* **13**, 1430–1437 (2004).
8. E. Feldman and J. Aboudi, Buckling analysis of functionally graded plates subjected to uniaxial loading, *Compos. Struct.* **38**, 29–36 (1997).

9. K. D. Kim, G. R. Lomboy and S. C. Han, Geometrically non-linear analysis of functionally graded material (FGM) plates and shells using a four node quasi-conforming shell element, *J. Compos. Mater.* **42**, 485–511 (2008).
10. L. S. Ma and T. J. Wang, Relationships between axisymmetric bending and buckling solutions of FGM circular plates based on third-order plate theory and classical plate theory, *Intl J. Solids Struct.* **41**, 85–101 (2004).
11. A. M. Afsar, R. Rahman, Y. Q. Wang, Y. Shi and J. I. Song, Finite difference solution of stress and strain in an FGM plate, in: *Proc.16th Ann. Intl Conf. Composites/Nano Engineering — ICCE-16*, Kunming, China (2008).
12. Y. N. Chung and H. X. Chang, Mechanical behavior of rectangular plates with functionally graded coefficient of thermal expansion subjected to thermal loading, *J. Therm. Stresses* **31**, 368–388 (2008).
13. Y. Obata and N. Noda, Steady thermal stresses in a hollow circular cylinder and a hollow sphere of a functionally gradient material, *J. Therm. Stresses* **17**, 471–487 (1994).
14. K. M. Liew, S. Kitipornchai, X. Z. Zhang and C. W. Lim, Analysis of the thermal stress behavior of functionally graded hollow circular cylinders, *Intl J. Solids Struct.* **40**, 2355–2380 (2003).
15. T. Mura, *Micromechanics of Defects in Solids: Mechanics of Elastic and Inelastic Solids*. Kluwer Academic Publishers, Dordrecht, The Netherlands (1987).
16. A. M. Afsar and H. Sekine, Optimum material distributions for prescribed apparent fracture toughness in thick-walled FGM circular pipes, *Intl J. Press. Vessels Pip.* **78**, 471–484 (2001).
17. A. M. Afsar and M. Anisuzzaman, Stress intensity factors of two diametrically opposed edge cracks in a thick-walled functionally graded material cylinder, *Engng Fract. Mech.* **74**, 1617–1636 (2007).
18. A. M. Afsar, M. Anisuzzaman and J. I. Song, Inverse problem of material distribution for desired fracture characteristics in a thick-walled functionally graded material cylinder with two diametrically-opposed edge cracks, *Engng Fract. Mech.* **76**, 845–855 (2008).
19. A. N. Eraslan and T. Akis, The stress response of partially plastic rotating FGM hollow shafts: analytical treatment for axially constrained ends, 1, *Mech. Based Designed Struct. Machines* **34**, 241–260 (2006).
20. A. M. Zenkour, Stress distribution in rotating composite structures of functionally graded solid disks, *J. Mater. Process. Technol.* (2008) (in press).
21. J. R. Cho and H. J. Park, High strength FGM cutting tools: finite element analysis on thermoelastic characteristics, *J. Mater. Process. Technol.* **130–131**, 351–356 (2002).
22. B.-O. Sallai, A. Tounsi, I. Mechab, B. M. Bachir, M. Meradjah and B. E. A. Adda, A theoretical analysis of flexional bending of Al/Al_2O_3 S-FGM thick beams, *Comput. Mater. Sci.* (2008) (in press).
23. S. P. Timoshenko and J. N. Goodier, *Theory of Elasticity*, 3rd edn. McGraw-Hill Book Company, New York, USA (1970).